Numerical calculation of the optical absorption in semiconductor quantum structures

S. Glutsch* and D. S. Chemla
Department of Physics, University of California, Berkeley, California 94720
and Material Sciences Division, Lawrence Berkeley National Laboratory, Berkeley, California 94720

F. Bechstedt
Friedrich-Schiller-Universität, Institut für Festkörpertheorie und Theoretische Optik, Max-Wien-Platz 1, 07743 Jena, Germany
(Received 17 January 1996; revised manuscript received 12 April 1996)

We describe a highly efficient, general-purpose, and easy-to-use method of calculating the optical absorption of semiconductor microstructures. The linear optical susceptibility is obtained by the numerical evaluation of the polarization in real space and real time, using finite differences and the leap-frog scheme. Numerical effort and storage scale as $O(N)$, where N is the number of base elements. The algorithm is suitable for large-scale quantum systems. For illustration, we apply this method to quantum wells in a perpendicular magnetic field, flat quantum dots, superlattices, coupled multiple quantum wells, and excitons on rough interfaces. [S0163-1829(96)04339-1]

I. INTRODUCTION

The physics of low-dimensional semiconductors has evolved rapidly during the past two decades.[1] Quantum wells, superlattices, quantum wires, quantum dots, polymers, and nanocrystals are examples of those materials.

The optical properties of semiconductors are determined by eigenvalues and eigenvectors of the electron-hole motion.[2] Besides the Coulomb attraction between electron and hole, and the quantum confinement, this motion can also be under the influence of electric or magnetic fields, interface roughness, and impurities. The configuration space is generally a six-dimensional domain in real (Wannier) or momentum (Bloch) space, and the wave function may have multiple components due to spin and band quantum numbers. Thus, in most cases of practical interest, the optical properties are calculated numerically.

The number of base functions N required for a numerical treatment can reach huge values, typically a million. Obviously, those large-scale systems cannot be treated with standard eigenroutines where the full matrix with N^2 elements has to be stored and the numerical effort scales like N^3. The dimension which can be handled that way is limited to about 10 000 by memory and computing time.[3] For larger sets of base functions, iterative diagonalizations, based on the Lanczos algorithm, have been successfully used.[4,7]

An alternative approach is to express the Coulomb Green's function in terms of an inverse operator.[5,6,8] Then a boundary-value problem has to be solved for each frequency. The differential operator is neither Hermitian and positive definite, nor diagonal dominant, as required by most matrix iterations. For one-dimensional domains, however, the band-diagonal set of equations can be solved exactly in $O(N)$ operations with $O(N)$ variables to be stored. As the dimensionality increases, the computational effort approaches $O(N^3)$ and the memory $O(N^2)$. Yet the solution of the boundary-value problem can still be efficient for strongly anisotropic domains, and calculations with 50 000 base functions have been reported.[9]

There is a long tradition in the numerical solution of initial-value problems.[10,11] Although only a very few publications explicitly deal with the Schrödinger equation, the methods are very general and can be applied to this problem, too. During the past 15 years, wave-packet propagation has been studied numerically, mostly in atomic and molecular physics.[12–14]

It is very common in semiconductor physics to use the eigenfunctions of the interaction-free electron-hole pair as base elements.[4,6,15] This results in a tedious evaluation of integrals for Coulomb matrix elements. The representation in real space can be more efficient, and has recently been applied with much success in electronic-structure calculations.[16]

In this paper, we present a highly efficient method for calculating the optical spectrum of semiconductor microstructures which is based on a real-space representation of the Hamiltonian, and the time-dependent solution of the Schrödinger equation. In Sec. II, we derive the formulation of the optical susceptibility as an initial-value problem. Finite-difference schemes for the solution of the time-dependent Schrödinger equation are evaluated in Sec. III. In Sec. IV, the described method is applied to various kinds of low-dimensional systems such as quantum wells, quantum dots, superlattices, coupled quantum wells, and rough interfaces, with up to four million base functions. A summary is given in Sec. V.

II. THE LINEAR OPTICAL SUSCEPTIBILITY OF LOW-DIMENSIONAL SEMICONDUCTOR STRUCTURES

The interaction of a semiconductor with an optical field is described by the semiconductor Bloch equations.[17] The electron-hole pair amplitude, linearized in the field, obeys an inhomogeneous Schrödinger equation. In the effective-mass approximation and real-space representation, it takes the form

$$i\hbar\left(\frac{\partial}{\partial t}+\gamma\right)\psi(\mathbf{r}_e,\mathbf{r}_h,t)=\Bigg[-\frac{1}{2m_e}\left|\frac{\hbar}{i}\nabla_e+e\mathbf{A}(\mathbf{r}_e)\right|^2 -\frac{1}{2m_h}\left|\frac{\hbar}{i}\nabla_h-e\mathbf{A}(\mathbf{r}_h)\right|^2 +U_e(\mathbf{r}_e)+U_h(\mathbf{r}_h) -\frac{e^2}{4\pi\varepsilon_0\varepsilon|\mathbf{r}_e-\mathbf{r}_h|}\Bigg]\psi(\mathbf{r}_e,\mathbf{r}_h) -\mu\,\delta(\mathbf{r}_e-\mathbf{r}_h)E(t), \tag{1}$$

where

$$\psi(\mathbf{r}_e,\mathbf{r}_h,-\infty)=0.$$

The inhomogeneity (source term) is determined by the electric field E and the dipole matrix element μ. The meanings of the other symbols are as follows: γ — homogeneous linewidth (dephasing constant); $m_{e,h}$ — effective masses of electron and hole, respectively; $-e$ — electron charge; $\mathbf{A}$ — vector potential of the magnetic field; $U_{e,h}$ — confinement potentials of electrons and holes, respectively; $\varepsilon_0=8.85419$ As/(Vm) — vacuum dielectric constant; and ε — relative background dielectric constant of the semiconductor.

The electron-hole-pair amplitude gives rise to a macroscopic polarization (dipole density),

$$P(t)=\frac{1}{\Omega}\mu^*\int d^3\mathbf{r}\;\psi(\mathbf{r},\mathbf{r},t), \tag{2}$$

where Ω is the normalization volume (area, length). Due to the linear nature of Eq. (1), the Fourier transform of the polarization,

$$\widetilde{P}(\omega)=\int_{-\infty}^{+\infty}dt\;e^{+i\omega t}P(t),$$

is proportional to the Fourier transform of the electric field $\widetilde{E}$. This relationship is expressed in the definition of the linear optical susceptibility:

$$\chi(\omega)=\frac{\widetilde{P}(\omega)}{\varepsilon_0\widetilde{E}(\omega)}. \tag{3}$$

In most cases, the differential operator in Eq. (1) reveals symmetries. Then, using appropriate coordinates, the actual number of variables can be reduced to less than six, and, technically, Eqs. (1) and (2) take a different form. In order to obtain a more general notation, we assume that ψ is defined on an α-dimensional domain G with a measure $dG=d\xi_1\cdots d\xi_\alpha\;g(\xi_1,\ldots,\xi_\alpha)$, where $g(\boldsymbol{\xi})>0$ almost everywhere. The scalar product

$$\langle\varphi|\psi\rangle=\int_G dG\,\varphi^*(\boldsymbol{\xi})\psi(\boldsymbol{\xi}) \tag{4}$$

defines a Hilbert space of functions defined on G and implies a norm $\|\|$.

With the above definitions, Eqs. (1) and (2) take the form

$$i\hbar\left(\frac{d}{dt}+\gamma\right)|\psi(t)\rangle-\hat{H}|\psi(t)\rangle=-E(t)|\mu\rangle,\qquad |\psi(-\infty)\rangle=|0\rangle \tag{5}$$

and

$$P(t)=\langle\mu|\psi(t)\rangle, \tag{6}$$

respectively. The operator $\hat{H}$ is Hermitian, and the remaining prefactors are contained in the definition of $|\mu\rangle$. The formulation (5–6) of the problem is very general, and is not restricted to the effective-mass approximation. It also applies for complicated valence band structures,[15] molecules,[18] and semiconductor nanocrystals.[19] In nonlinear optics, the problem is solved perturbatively. In that case, each order of the density matrix obeys an equation of the same type as Eq. (5), with the inhomogeneity determined by its lower orders and the electric field.

To obtain the optical susceptibility (3), Eqs. (5) and (6) can be solved using the Fourier transform. This leads to the usual representations

$$\chi(\omega)=\sum_\lambda\frac{|\langle\mu|\varphi_\lambda\rangle|^2}{E_\lambda-\hbar(\omega+i\gamma)}, \tag{7}$$

with

$$\hat{H}|\varphi_\lambda\rangle=E_\lambda|\varphi_\lambda\rangle;\quad \langle\varphi_\lambda|\varphi_{\lambda'}\rangle=\delta_{\lambda\lambda'};\quad \sum_\lambda|\varphi_\lambda\rangle\otimes\langle\varphi_\lambda|=\hat{I}$$

and

$$\chi(\omega)=\langle\mu|[\hat{H}-\hbar(\omega+i\gamma)\hat{I}]^{-1}|\mu\rangle. \tag{8}$$

The symbol $\hat{I}$ represents the identity operator. From Eq. (7), it follows that the optical susceptibility is discontinuous with respect to γ, at $\gamma=0$. The function $\mathrm{Im}\chi(\omega)$ in the limit $\gamma\to+0$ is called the optical density.

As an alternative to the eigenvalue problem (7) or the boundary-value problem (8), we trace back the optical susceptibility to an initial-value problem, viz.,

$$\chi(\omega)=\frac{1}{-i\hbar}\int_0^\infty dt e^{-i\omega t}e^{-\gamma t}\langle\mu|\psi(t)\rangle, \tag{9}$$

where

$$i\hbar\frac{d}{dt}|\psi(t)\rangle=\hat{H}|\psi(t)\rangle;\quad |\psi(0)\rangle=|\mu\rangle. \tag{10}$$

Since $|\psi(t)\rangle=\exp[\hat{H}t/(i\hbar)]|\mu\rangle$, this is equivalent to Eq. (8). Equations (9–10) can also be obtained by choosing $E(t)=-i\hbar\,\delta(t)$ as the right-hand side of the inhomogeneous Schrödinger equation (5).

In practice, the upper limit of the Fourier integral (9) can be truncated at a finite value $t_{\max}=5/\gamma$, since $e^{-5}=0.006\,73\ldots$ Then, the remaining task is to solve the initial-value problem (10) in the interval $[0,\,t_{\max}]$. In the next section, we discuss finite-difference schemes for the solution of Eq. (10) and we address the issues of accuracy, stability, numerical effort, storage, and implementation.

III. NUMERICAL SOLUTION

A simple-minded numerical approach of Eq. (10), e.g., solving a set of ordinary differential equations with a fully $N\times N$ coefficient matrix H by means of a Runge-Kutta method, would result in $O(N^2 t_{\max}^2 \|H\|^2/\hbar^2)$ floating-point operations, where $\|H\|$ is the norm of H. However, using a sparse matrix and a stable propagation scheme in the time domain, the computational effort can be reduced to $O(Nt_{\max}\|H\|/\hbar)$.

Sparse matrices are either obtained from finite-element methods or from finite differencing. Besides polynomial approximations for large time steps, there are basically two difference schemes used for the time evolution of Schrödinger equations: the operator splitting method and the leap-frog scheme. We chose finite differences combined with the leap-frog method. As a fully explicit scheme in space and time, it is the easiest to implement and most efficient on vector machines.

A. Discretization in space

Now, we discretize the Schrödinger equation (10) in space, using finite differences. Since it is a standard technique, we only give a brief description of the basic concepts and expressions for those operators which will be used in the next section. For a comprehensive representation of the subject, we refer to mathematical literature.[10,11]

A function φ, defined on the domain G is characterized by its values $\varphi_j=\varphi(\boldsymbol{\xi}_j)$ on the grid $\{\boldsymbol{\xi}_j\}$, $j=1,\ldots,N$. The scalar product (4) is approximated by the quadrature formula,

$$\langle\varphi|\psi\rangle=\sum_{j=1}^{N}\varphi_j^* g_j\psi_j=(\vec{\varphi},\vec{\psi}),$$

with weights $g_j>0$. The symbols $\vec{\varphi}$ and $\vec{\psi}$ denote column vectors with components φ_j and ψ_j, respectively. In accordance with the above equation, the representation of the Dirac function, $D(\boldsymbol{\xi},\boldsymbol{\xi}')=\delta(\boldsymbol{\xi}-\boldsymbol{\xi}')/g(\boldsymbol{\xi})$ is $D_{jj'}=\delta_{jj'}/g_j$, where $\boldsymbol{\xi}_{j'}=\boldsymbol{\xi}'$. For the discretization in time, it is essential that the matrix H, resulting from the discretization of the Hamiltonian $\hat{H}$, is Hermitian, with respect to the scalar product $(.,.)$ of the discrete space of grid functions.

We consider a one-dimensional domain $G=[a,b]$ with a weight function $g(x)\equiv 1$. A discretization of the operator $\Delta=\partial^2/\partial x^2$ is given by

$$(\Delta\varphi)_j=\frac{\varphi_{j-1}-2\varphi_j+\varphi_{j+1}}{h^2}.$$

The resulting matrix is Hermitian for $g_i\equiv h$. Vanishing boundary conditions, i.e., $\varphi(a)=0$ and $\varphi(b)=0$, lead to $x_j=jh$, $h=(b-a)/(N+1)$, $j=1,\ldots,N$, $\varphi_0=0$, and $\varphi_{N+1}=0$. For cyclic (or periodic) boundary conditions, $\varphi(a)=\varphi(b)$ and $\varphi'(a)=\varphi'(b)$, we have $x_j=jh$, $h=(b-a)/N$, $j=0,\ldots,N-1$, and $\varphi_{N+j}=\varphi_j$. In this case, the largest eigenvalue in magnitude is $-4/h^2$, which is the same as for vanishing boundary conditions, in the limit $N\to\infty$.

Now, we consider the radial part of the two-dimensional Laplacian,

$$\Delta=\frac{1}{\rho}\frac{\partial}{\partial\rho}\left(\rho\frac{\partial}{\partial\rho}\right),$$

on the domain $G=[0,R]$; $g(\rho)=\rho$ with the boundary condition $\varphi(R)=0$. A discretization is given by

$$(\Delta\varphi)_j=\frac{1}{\rho_j}\frac{\rho_{j-1/2}\varphi_{j-1}-2\rho_j\varphi_j+\rho_{j+1/2}\varphi_{j+1}}{h^2}$$

$$\text{for } j=1,\ldots,N-1,$$

$$(\Delta\varphi)_0=4\frac{\varphi_1-\varphi_0}{h^2};\quad \rho_{j\pm1/2}=(j\pm\tfrac{1}{2})h,$$

where $\rho_j=jh$, $h=R/N$, $j=0,\ldots,N-1$, and $\varphi_N=0$. The corresponding matrix is Hermitian for $g_0=\frac{1}{8}h$, $g_j=jh$, $j=1,\ldots,N-1$. Laplacians in many dimensions can be constructed from one-dimensional Laplacians.

The potentials encountered in the description of low-dimensional semiconductors can take various forms. Infinite barriers lead to vanishing boundary conditions in the confinement directions. If a potential U is uniformly bound, it can be discretized according to $(U\varphi)_j=U_j\varphi_j$; $U_j=U(\boldsymbol{\xi}_j)$.

A potential may have an integrable singularity, still leading to a finite value of the wave function. Some authors circumvent this difficulty by transforming the wave function to be zero at this point, thus obtaining an additional boundary condition,[14] or defining a grid which does not contain the singularity.[12] However, this results in a loss of accuracy if the electron-hole-pair amplitude is to be calculated at the singularity. The use of non-equidistant grid points would make the method less flexible. A more convenient way is to use the ground-state wave function and energy: if $-\frac{1}{2}\Delta\varphi_{\text{g.s.}}(\boldsymbol{\xi})+V(\boldsymbol{\xi})\varphi_{\text{g.s.}}(\boldsymbol{\xi})=E_{\text{g.s.}}\varphi_{\text{g.s.}}(\boldsymbol{\xi})$ and $\varphi_{\text{g.s.}}(\boldsymbol{\xi})\neq 0$ for $\boldsymbol{\xi}\in G$, then

$$V_j=\frac{\frac{1}{2}(\Delta\varphi_{\text{g.s.}})_j}{\varphi_{\text{g.s.}j}}+E_{\text{g.s.}} \tag{11}$$

is a discretization of the potential V.

With the above techniques, we successfully discretized the Hamiltonian $\hat{H}$. The resulting $N\times N$ matrix H is sparse, i.e., only $O(N)$ of its elements are different from zero. All eigenvalues are real, and the eigenvectors are orthogonal, i.e.,

$$H\vec{\varphi}_\lambda=E_\lambda\vec{\varphi}_\lambda;\quad (\vec{\varphi}_\lambda,\vec{\varphi}_{\lambda'})=\delta_{\lambda\lambda'}. \tag{12}$$

The norm (or spectral radius) of H, defined as $\|H\|=\sup(\|H\varphi\|/\|\varphi\|)$; $\vec{\varphi}\neq\vec{0}$, is related to the eigenvalues by $\|H\|=\max\{|E_1|,\ldots,|E_N|\}$.

B. Discretization in time

After having performed the discretization in space in the last subsection, the initial-value problem (10) transforms into a linear set of differential equations,

$$i\hbar \frac{\partial}{\partial t}\vec{\psi}(t)=H\vec{\psi}(t). \tag{13}$$

Since H has been found to be sparse, it is desirable to solve Eq. (13) by a direct method so that only the operation $\vec{\psi} \mapsto H\vec{\psi}$, which requires $O(N)$ operations, has to be carried out for each time step. This can be done by the following difference scheme:

$$i\hbar \frac{\vec{\psi}(t_{n+2})-\vec{\psi}(t_n)}{2\Delta t}=H\vec{\psi}(t_{n+1}); \quad t_n=n\Delta t, \tag{14}$$

which is called the central difference or ''leap-frog'' method.[11,13,14]

Now, we determine the step size Δt for which the above recursion is stable. Therefore, we expand $\vec{\psi}$ on the eigenvectors (12) of H according to

$$\vec{\psi}(t_n)=\sum_{\lambda=1}^{N} \psi_\lambda(t_n)\vec{\varphi}_\lambda .$$

For each $\lambda=1,\ldots,N$, the sequence $\{\psi_\lambda(t_n)\}$ obeys the three-level recursion formula (14), where the matrix H has been replaced by its eigenvalue E_λ. Its fundamental solutions are $(\omega_\lambda=E_\lambda/\hbar)$:

$$\psi_\lambda^{\pm}(t_n)=\begin{cases}[-i\omega_\lambda\Delta t\pm\sqrt{1-(\omega_\lambda\Delta t)^2}]^n & \text{for } \omega_\lambda\Delta t\neq 1\\ (1\pm n)(-i)^n & \text{for } \omega_\lambda\Delta t=1\end{cases}. \tag{15}$$

Hence, the difference scheme (14) is stable, i.e., $\|\vec{\psi}(t_n)\|$ is uniformly bound, if $\Delta t<\hbar/\|H\|$.

The solution for $\vec{\psi}$ follows from the homogeneous solutions (15) and the initial condition, $\vec{\psi}(0)=\vec{\mu}$. Since the three-level recursion (14) requires two initial values, we have to generate $\vec{\psi}(t_1)$ from $\vec{\psi}(t_0)$, consistently with the differential equation (13). This can be done by an explicit Euler step, $\vec{\psi}(t_1)=(I-iH\Delta t/\hbar)\vec{\psi}(t_0)$. Then, in the stability region, the solution is

$$\vec{\psi}(t_n)=\sum_{\lambda=1}^{N}(c_\lambda^{+}e^{-i\omega_\lambda^{+}t_n}+c_\lambda^{-}e^{-i\omega_\lambda^{-}t_n})(\vec{\varphi}_\lambda,\vec{\mu})\vec{\varphi}_\lambda ,$$

where

$$c_\lambda^{+}=\frac{1+\sqrt{1-(\omega_\lambda\Delta t)^2}}{2\sqrt{1-(\omega_\lambda\Delta t)^2}}; \quad c_\lambda^{-}=1-c_\lambda^{+};$$

$$\omega_\lambda^{+}=\frac{\arcsin(\omega_\lambda\Delta t)}{\Delta t}; \quad \omega_\lambda^{-}=\frac{\pi}{\Delta t}-\omega_\lambda^{+}.$$

Let us briefly summarize the features of the method (14) which are most important for our physical problem. The amplitudes $c_\lambda^{\pm}$ are real. This is important in situations where the real part of the optical susceptibility is divergent and must not be mixed with the finite imaginary part. The deviation of the c_λ^{+} from unity is $O[(\omega_\lambda\Delta t)^2]$ for $\omega_\lambda\Delta t\to 0$. There is no numerical damping introduced if Δt is in the stability region. The relative error of the frequencies ω_λ^{+} compared to the true values ω_λ is $O[(\omega_\lambda\Delta t)^2]$. Usually, the norm of H already enforces a sufficiently small step size Δt and thus ensures accurate propagation of the lower eigenmodes. The frequencies ω_λ^{+} are located in the interval $(-\pi/2/\Delta t,+\pi/2/\Delta t)$, whereas the numerical artifacts ω_λ^{-} are all situated outside this region. This is a big advantage over the operator-splitting method, where the errors originate from noncommutativity of operators and can be distributed over the whole frequency range.

C. Storage, computational efforts, and implementation

Since we deal with large-scale systems, storage and computational efforts are given in the limit $N\to\infty$. The number of complex variables is between $2N$ and $4N$, depending on whether two or three time levels are stored and if the potential is precalculated or not.

If the calculation of $\vec{\psi}(t_{n+2})$ from $\vec{\psi}(t_n)$ and $\vec{\psi}(t_{n+1})$ requires kN floating-point operations, then the total number of floating-point operations is $5kN\|H\|/(\hbar\gamma)$. It is worth noting that the computing speed is not only determined by the nominal numerical effort, but depends on efficient implementations, too. Equation (14) is entirely built upon vector additions and matrix-vector multiplications, and can be directly vectorized.

The implementation is very straightforward and does not employ variable data structures and recursive calls. Besides a fast Fourier transform, no library routines have to ''make work.'' The FORTRAN programs used in the next section are all shorter than 400 lines in total. In all cases, it took less than one day to customize the program to a new situation, for example, to add or remove space directions, and to exchange Laplacians, boundary conditions, or potentials.[20]

IV. EXAMPLES

The main purpose of this section is to demonstrate the usefulness of the described numerical method. The examples also show how the abstract notations in Secs. II and III work, in practice. They cover one-, two-, three-, and four-dimensional domains, Cartesian and cylindrical coordinates, vanishing and periodic boundary conditions. Out of a large class of problems which could be treated, we choose those which have not yet been comprehensively studied and only partial results have been published, namely, quantum wells with finite thickness in a perpendicular magnetic field, flat quantum dots, superlattices, multiple quantum wells, and excitons on rough interfaces.

Dimensionless quantities are obtained by choosing $\hbar=m=e^2/(4\pi\varepsilon_0\varepsilon)=1$ in Eq. (1), where $m=m_e m_h/(m_e+m_h)$ is the reduced mass. This leads to the Hartree units $E^*=me^4/[(4\pi\varepsilon_0\varepsilon)^2\hbar^2]$ and $a^*=4\pi\varepsilon_0\varepsilon\hbar^2/(me^2)$ for energy and length, respectively. For Gallium Arsenide we have approximately $E^*=9.4$ meV and $a^*=12$ nm.

To obtain a formulation which is independent of the energy gap, we either subtract the ''bottom'' of the band edge or, when it was appropriate, the energy of the lowest subband pair. Since we are mainly interested in qualitative re-

sults, we assume equal masses for electron and hole. The effect of different masses is discussed elsewhere.[21] Except for multiple quantum structures, where tunneling through the barriers essentially modifies the optical spectrum, we assume infinitely high barriers, which lead to vanishing boundary conditions. The Coulomb potential is discretized according to Eq. (11) with $\varphi_{\mathrm{g.s.}}(x,y,z)=\exp(-\sqrt{x^2+y^2+z^2})$; $E_{\mathrm{g.s.}}=-\frac{1}{2}$ in three dimensions and $\varphi_{\mathrm{g.s.}}(x,y)=\exp(-2\sqrt{x^2+y^2})$; $E_{\mathrm{g.s.}}=-2$ in two dimensions.

The homogeneous broadening is fixed at $\gamma=0.1$. The time step Δt is chosen such that the condition of stability is fulfilled and that $t_{\max}/\Delta t$ is an integer power of 2. In the following examples, the number of steps was between 2^{12} and 2^{15}.

A. Ideal quantum well

In an ideal quantum well, the electron-hole motion is restricted to a two-dimensional plane. This model is used for the description of thin quantum wells, and has been treated analytically and numerically many times. We calculate the optical spectrum numerically to check the accuracy of our numerical approach. In Cartesian coordinates, the Hamiltonian $\hat{H}$, the dipole matrix element μ, the domain G, and the weight function g are

$$(\hat{H}\psi)(x,y)=\left[-\frac{1}{2}\frac{\partial^2}{\partial x^2}-\frac{1}{2}\frac{\partial^2}{\partial y^2}-\frac{1}{\sqrt{x^2+y^2}}+\frac{1}{8}\omega_c^2(x^2+y^2)\right]\psi(x,y),$$

$$\mu(x,y)=\delta(x)\delta(y);\quad G=\left[-\frac{L}{2},+\frac{L}{2}\right]^2;\quad g(x,y)\equiv 1.$$

Here, $\omega_c=eB/m$ is the cyclotron frequency of an applied perpendicular magnetic field B. We use periodic boundary conditions in the x and y direction with a normalization length $L=200$ and mesh sizes $h=\frac{1}{8}$ in the x and y direction. A comparable accuracy can be expected from a solution in polar coordinates,

$$(\hat{H}\psi)(\rho)=\left[-\frac{1}{2}\frac{1}{\rho}\frac{\partial}{\partial\rho}\left(\rho\frac{\partial}{\partial\rho}\right)-\frac{1}{\rho}+\frac{1}{8}\omega_c^2\rho^2\right]\psi(x,y),$$

$$\mu(\rho)=\frac{\delta(\rho)}{2\pi\rho};\quad G=[0,R];\quad g(\rho)=2\pi\rho,$$

with $R=141$ and the same mesh size $h=\frac{1}{8}$.

In Fig. 1(a), the optical absorption of a two-dimensional semiconductor for zero magnetic field is plotted on a logarithmic scale. The exact solution (solid line) is compared with the numerical solution in Cartesian (dashed line) and in polar coordinates (dotted line). The continuum absorption is slightly overemphasized in the numerical solution. Besides this fact, the agreement is very good.

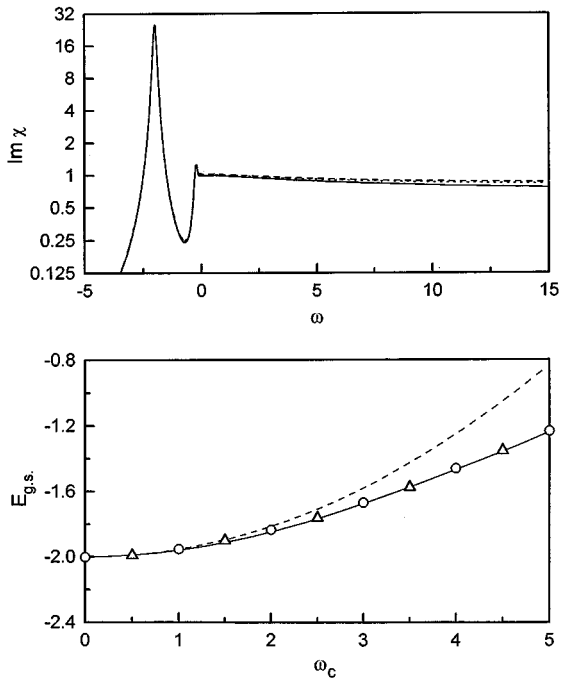

FIG. 1. Top: imaginary part of the optical susceptibility for an ideal quantum well on a logarithmic scale vs frequency. Solid line — exact solution; dashed line — numerical solution in Cartesian coordinates; dotted line — numerical solution in polar coordinates. Bottom: ground-state energy of a two-dimensional magnetoexciton vs cyclotron frequency. Solid line — exact solution; dashed line — diamagnetic shift; circles — numerical solution in Cartesian coordinates; triangles — numerical solution in polar coordinates.

To study the accuracy of the discretization (11) of the Coulomb potential, we take into account a perpendicular magnetic field which manifests itself by an additional parabolic potential. The ground-state energy $E_{\mathrm{g.s.}}$ is plotted in Fig. 1(b). The exact solution (solid line) is compared with the numerical solution in Cartesian (circles) and polar (triangles) coordinates. Up to high magnetic fields (GaAs: $\omega_c\approx 0.32\,B/\mathrm{T}$), the agreement is excellent. In the low-field limit, $\omega_c\to 0$, the ground-state energy behaves like $E_{\mathrm{g.s.}}\sim -2+\frac{3}{64}\,\omega_c^2$ (dashed line). This result follows from perturbation theory and is known as a diamagnetic shift.

From this case study, we conclude that reliable results can be obtained from the chosen mesh sizes and the normalization lengths in the directions of free motion. Unless stated otherwise, we assume normalization lengths of 200 and 141 for Cartesian and polar coordinates, respectively, and a mesh size of $\frac{1}{8}$. If a dimension is smaller than 1, a minimum of seven grid points is used.

B. Quantum well with finite thickness in a perpendicular magnetic field

Extensive theoretical studies in the past were devoted to ideal two-dimensional magnetoexcitons or to the ground-state energy of magnetoexcitons in a quantum well. Here, we perform a transition from two-dimensional magnetoexcitons to three-dimensional magnetoexcitons.

We consider a quantum well with thickness d in a magnetic field. The optical susceptibility is determined by

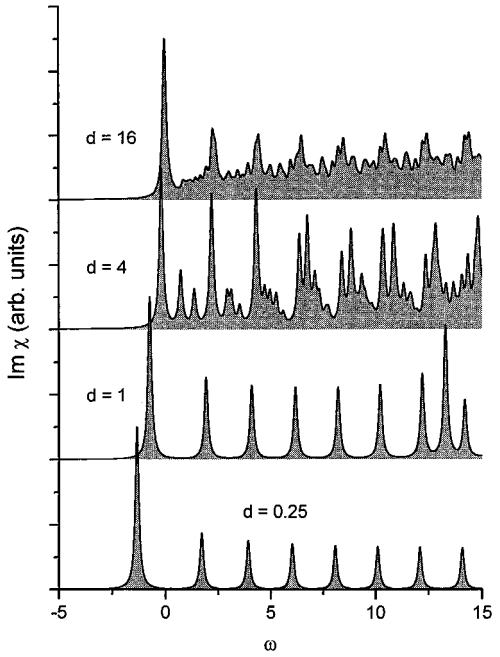

FIG. 2. Optical absorption of a quantum well in a perpendicular magnetic field with cyclotron frequency $\omega_c=2$. The well thicknesses are $d=0.25$, 1, 4, and 16.

$$(\hat{H}\psi)(\rho,z_e,z_h)$$
$$=\left[-\frac{1}{2}\frac{1}{\rho}\frac{\partial}{\partial\rho}\left(\rho\frac{\partial}{\partial\rho}\right)-\frac{1}{4}\frac{\partial^2}{\partial z_e^2}-\frac{1}{4}\frac{\partial^2}{\partial z_h^2}-\frac{\pi^2}{2d^2}\right.$$
$$\left.+\frac{1}{8}\omega_c^2\rho^2-\frac{1}{\sqrt{\rho^2+(z_e-z_h)^2}}\right]\psi(\rho,z_e,z_h),$$

$$\mu(\rho,z_e,z_h)=\frac{1}{\sqrt{d}}\frac{\delta(\rho)}{2\pi\rho}\delta(z_e-z_h);$$

$$G=[0,R]\times[0,d]^2;\quad g(\rho,z_e,z_h)=2\pi\rho.$$

For a fixed cyclotron frequency $\omega_c=2$, we chose $R=10$, which is about 14 times the magnetic length.

Figure 2 shows the optical spectrum for a well thickness $d=0.25$, 1, 4, and 16. The cyclotron frequency is fixed at $\omega_c=2$. The spectrum of a thin quantum well resembles that of the ideal two-dimensional case[22] with discrete transition energies. Except for the lowest one, they are separated from each other by approximately the cyclotron frequency. An intermixing with excited quantum-well states occurs as the thickness is increased. The spectrum is fairly irregular when the magnetic and the size quantization are of the same order of magnitude. Finally, for large thickness, the absorption profile turns into that of a bulk semiconductor in a magnetic field with characteristic Fano resonances for higher-order magnetoexciton states.[23] Interestingly, the signatures of the confinement in the growth direction are observed even for very thick samples, which are usually referred to as ''bulk'' semiconductors.[24]

C. Quantum dots

We focus on quantum dots, which were fabricated on the basis of a quantum well. Flat, square quantum dots have been studied experimentally by Brunner *et al.*[25] The Hamiltonian, the dipole matrix element, the domain, and the weight function are

$$(\hat{H}\psi)(x_e,x_h,y_e,y_h)=\left(-\frac{1}{4}\frac{\partial^2}{\partial x_e^2}-\frac{1}{4}\frac{\partial^2}{\partial x_h^2}-\frac{1}{4}\frac{\partial^2}{\partial y_e^2}-\frac{1}{4}\frac{\partial^2}{\partial y_h^2}\right.$$
$$\left.-\frac{\pi^2}{b^2}-\frac{1}{\sqrt{(x_e-x_h)^2+(y_e-y_h)^2}}\right)$$
$$\times\psi(x_e,y_e,x_h,y_h),$$

$$\mu(x_e,y_e,x_h,y_h)=\frac{1}{b}\delta(x_e-x_h)\delta(y_e-y_h);$$

$$G=[0,b]^4;\quad g(x_e,x_h,y_e,y_h)\equiv 1,$$

where b is the length of the side.

The results of the calculation are shown in Fig. 3 for $b=2$, 3, 4, and 5. The spectrum of large quantum dots is quasicontinuous, i.e., the separation of the individual peaks is smaller than the homogeneous broadening. For $b=5$, the binding energy is close to the binding energy of the two-dimensional Coulomb potential, and the slope of the spectrum resembles the spectrum of a quantum well (dashed line). The spectra of the small dots are characterized by well-separated absorption peaks with different amplitudes and an increased binding energy.

D. Superlattices

Absorption spectra of superlattices have been calculated by Chang and co-workers,[4,7] using the **k**-space sampling

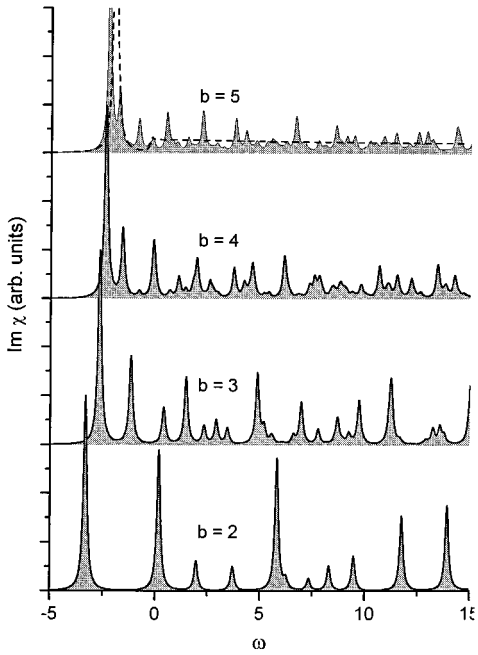

FIG. 3. Optical absorption of flat, square quantum dots with sides of length $b=2$, 3, 4, and 5.

method combined with an iterative diagonalization. The problem was also attacked by Whittaker,[8] solving a boundary-value problem. His model, however, only accounts for a single miniband pair. In our approach, no restriction is made with respect to the number of minibands. This allows us to perform a transition, from a bulk semiconductor to a superlattice and from a superlattice to a quantum well, by increasing the band discontinuity. This corresponds to the experimental situation, for example, of different Al concentrations x in a GaAs/$Ga_{1-x}Al_xAs$ superlattice.

Let d be the period of the superlattice, and H the discontinuity of both the valence and the conduction band. The Hamiltonian, the dipole matrix element, the normalization volume, and the weight function are

$$(\hat{H}\psi)(\rho,Z,z)=\left[-\frac{1}{2}\frac{1}{\rho\partial\rho}\left(\rho\frac{\partial}{\partial\rho}\right)-\frac{1}{8}\frac{\partial^2}{\partial Z^2}-\frac{1}{2}\frac{\partial^2}{\partial z^2}+U(Z+\tfrac{1}{2}z)+U(Z+\tfrac{1}{2}z)-\frac{1}{\sqrt{\rho^2+z^2}}\right]\psi(\rho,Z,z),$$

$$U(z)=H\Theta\left[-\cos\left(\frac{2\pi z}{d}\right)\right];\quad \mu(\rho,Z,z)=\frac{1}{\sqrt{d}}\frac{\delta(\rho)}{2\pi\rho}\delta(z),$$

$$G=[0,R]\times[0,d]\times\left[-\frac{L_z}{2},+\frac{L_z}{2}\right];\quad g(\rho,Z,z)=2\pi\rho,$$

and Θ denotes the Heavyside function. As a consequence of the Bloch theorem, the wave-function obeys periodic boundary conditions with respect to the center-of-mass coordinate Z. We mention that only one sign has to be changed to obtain the optical spectrum of a type-II superlattice.[26] This is a big advantage over previous approaches, where the Hamiltonian was represented in terms of miniband envelope functions.[4,7,8]

The optical spectra are shown in Fig. 4 for a period $d=1$ and different band offsets $H=0$, 5, 10, 15, and 20. The corresponding intervals for the z coordinate are $L_z=200$, 60, 30, 20, and 15. In order to trace back the origin of the different peaks, the one-dimensional (miniband) density of states in the growth (z) direction is plotted as a dashed line.

The value $H=0$ corresponds to a pure three-dimensional semiconductor. The one-dimensional density of states has the typical Lorentz-broadened $1/\sqrt{\omega}$ form. For $H=5$, the density of states exhibits forbidden zones. The continuum absorption in the miniband regions is about the same as for the bulk semiconductor, whereas it drops to the two-dimensional value in the regions of miniband gaps. When the width of the miniband is of the order of the two-dimensional binding energy ($H=10\ldots15$), a saddle-point exciton can be observed which originates from the critical point of the density of states at the top of the miniband.[27] As the height of the barriers is further increased ($H=15\ldots20$), the first miniband reduces to a single energy level, and the absorption spectrum turns into that of a quantum well.

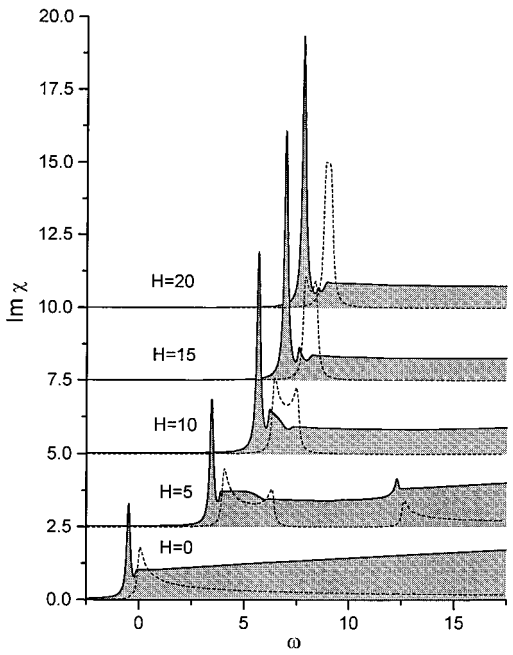

FIG. 4. Optical spectra of superlattices with a length of the period $d=1$ and barrier heights $H=0$, 5, 10, 15, and 20. The miniband density of states is marked as a dashed line.

E. Coupled quantum wells

A different approach to a superlattice is to start from a single quantum well and increase the number of periods p, thus obtaining a double, triple, etc., quantum well. In the limit $p\to\infty$, one should obtain the spectrum of a superlattice as calculated in the last subsection. Since any real superlattice consists of a finite number of layers, it is important to study the effects of the finite number of periods and to have an estimate when coupled quantum wells can be considered as a superlattice.

This time, Bloch symmetry cannot be assumed for the center-of-mass coordinate. Instead, the problem has to be formulated in terms of electron and hole coordinates z_e and z_h in the growth direction. This leads to

$$(\hat{H}\psi)(\rho,z_e,z_h)=\left[-\frac{1}{2}\frac{1}{\rho}\frac{\partial}{\partial\rho}\left(\rho\frac{\partial}{\partial\rho}\right)-\frac{1}{4}\frac{\partial^2}{\partial z_e^2}-\frac{1}{4}\frac{\partial^2}{\partial z_h^2}+U(z_e)+U(z_h)-\frac{1}{\sqrt{\rho^2+(z_e-z_h)^2}}\right]\psi(\rho,z_e,z_h),$$

$$\mu(\rho,z_e,z_h)=\frac{1}{\sqrt{L_z}}\frac{\delta(\rho)}{2\pi\rho}\delta(z_e-z_h),$$

$$G=[0,R]\times[0,L_z]^2;\quad L_z=(p-\tfrac{1}{2})d;$$

$$g(\rho,z_e,z_h)=2\pi\rho,$$

with the same potential U as in the last subsection. Vanishing boundary conditions are assumed for z_e and z_h, which means, physically, that the multiple quantum well is embedded in a material with virtually infinite band offset.

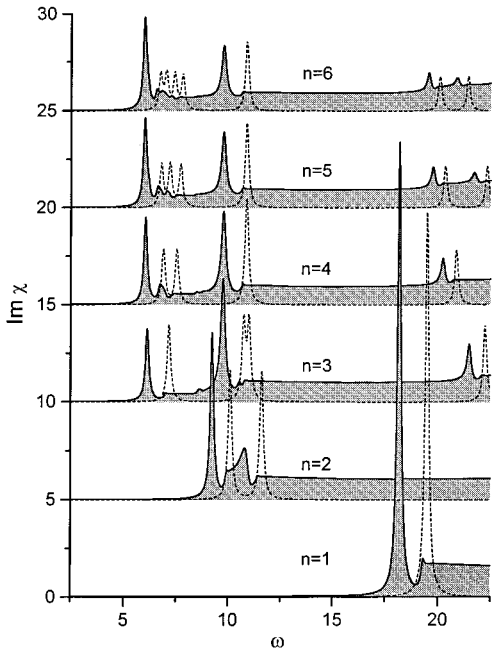

FIG. 5. Optical spectra of coupled quantum wells with a fixed barrier height $H=10$ and a number of periods $p=1$, 2, 3, 4, and 5. The one-dimensional density of states is marked as a dashed line.

The results of the calculation are shown in Fig. 5 for layer thickness $d=0.5$, a modulation depth $H=10$, and a number of periods $p=1,\ldots,6$. Again, the one-dimensional density of states, which is discrete this time, is shown as a dashed line.

A number of periods $p=1$ corresponds to a single quantum well with thickness $d=0.5$. In this case, the continuum starts at $\omega=\pi^2/(2\,d^2)=19.73\ldots$ For $p=2$, we observe two nearly degenerate excitons. The upper one is strongly coupled to the continuum of the lower one and, therefore, exhibits a pronounced Fano line shape. As the number of periods is further increased, a series of closely spaced absorption lines accumulates just above the ground state. These excitons are degenerate with continuum states and thus inhomogeneously broadened. The resulting quasicontinuum resembles the absorption profile in Fig. 4. There is also a pronounced Lorentzian peak at about $\omega=H$. Its height slightly decreases as the number of periods is increased. Interestingly, this feature is not found in the spectrum of the ideal superlattice, Fig. 4.

The nature of the peaks can be explained by means of the density of states. The lowest energy level of the quantization in z direction splits up into n different eigenvalues. The lowest $n-2$ eigenstates accumulate at the superlattice absorption edge, and a miniband is formed for $n\rightarrow\infty$. The upper two eigenstates, however, stay separate from the rest of the spectrum and their height disappears for $n\rightarrow\infty$. However, since they are weakly coupled to the continuum and their spectral weight decreases as $1/n$, they should be visible in real superlattices.

F. Rough interfaces

Schrödinger equations with stochastic potentials have been studied for many decades,[28] and are used to describe light scattering in inhomogeneous media, impurities, and optical properties of low-dimensional semiconductors with rough interfaces. Some one-dimensional potentials can be treated exactly, using the transfer matrix method.[28,29] Asymptotic expansions of the optical density can be performed in arbitrary dimensions, provided the moments A_m of the spectral density increase slower than $m!$.[30] This is useful only if all orders are known within some approximation and can be summed up analytically. In this subsection, we numerically calculate absorption spectra of excitons on rough interfaces, in one and two dimensions.

The optical absorption of an exciton under the influence of a rough interface in α dimensions is described by[29]

$$(\hat{H}\psi)(x,y)=\left[-\frac{1}{8}\frac{\partial^2}{\partial x_1^2}-\cdots-\frac{1}{8}\frac{\partial^2}{\partial x_\alpha^2}+W(x_1,\ldots,x_\alpha)\right]\psi(x_1,\ldots,x_\alpha),$$

$$\mu=\frac{1}{\sqrt{L_1\cdots L_\alpha}};\quad G=[0,L_1]\times\cdots\times[0,L_\alpha];\quad g\equiv 1.$$

The factor $\frac{1}{8}$ comes from the center-of-mass motion of the exciton and the fact that we have assumed equal masses for the electron and the hole. For $\alpha=1$, the above equation describes an exciton in a quantum wire with rough barriers, and $\alpha=2$ corresponds to an exciton in a quantum well with thickness fluctuations.

We study the influence of the fluctuations on the line shape for a Gaussian stochastic potential,[30]

$$W(\mathbf{r})=\frac{1}{\sqrt{L_1\cdots L_\alpha}}\sum_{\mathbf{k}\in 2\pi G^{-1}} e^{+i\mathbf{k}\cdot\mathbf{r}}|s(\mathbf{k})|e^{i\Phi(\mathbf{k})},$$

$$|s(\mathbf{k})|^2=\int d^\alpha\mathbf{k}\; e^{-i\mathbf{k}\cdot\mathbf{r}}A(\mathbf{r}),$$

$$\Phi(\mathbf{k})=\text{random}[-\pi,+\pi];\quad \Phi(-\mathbf{k})=-\Phi(\mathbf{k}).$$

The statistical properties of W are uniquely determined by the autocorrelation function $A(\mathbf{r}_1-\mathbf{r}_2)=\langle W(\mathbf{r}_1)W(\mathbf{r}_2)\rangle$. In our example, we assume $A(\mathbf{r})=H^2\exp[-r^2/(2\sigma^2)]$. The quantities H and σ can be interpreted as the depths and the correlation length of the fluctuations, respectively. The potential is self-averaging for $L_1,\ldots,L_\alpha\rightarrow\infty$, which means that the one calculation of $\chi(\omega)$ usually gives the same result as the statistical average $\langle\chi(\omega)\rangle$.

The calculation of the absorption spectra was done using a normalization length $L_x=131\,072$ in the one-dimensional case and $L_x=L_y=128$ in the two-dimensional case. The results are shown in Fig. 6 for parameters $H=0.5$ and $\sigma=0.125$, 0.25, 0.5, and 1. The classical limit, $\sigma\rightarrow\infty$, was obtained by convolution of the probability density $\langle\delta[\omega-V(\mathbf{r})]\rangle=(2\pi H^2)^{-1/2}\exp[-\omega^2/(2H^2)]$ with a Lorentzian $\gamma/(\omega^2+\gamma^2)$. In practice, this limit is reached if $1/(2\sigma^2)\ll H$. If both energies, $1/(2\sigma^2)$ and H, are of the same order of magnitude, a pronounced asymmetric line shape is observed: the maximum is shifted to a lower energy, and the high-energy shoulder decreases slower than in the classical limit. The full width at half maximum becomes

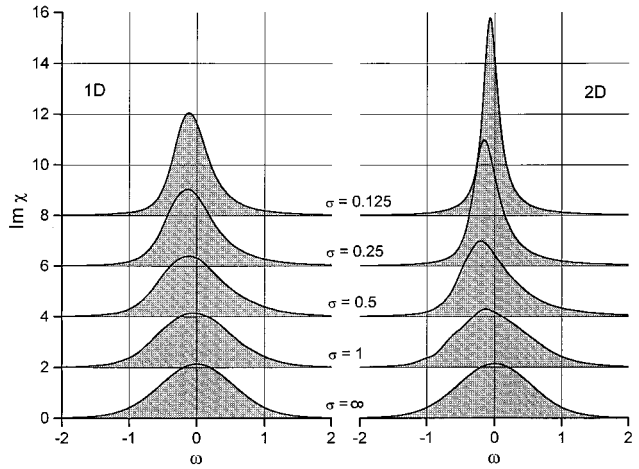

FIG. 6. Spectra of excitons on rough interfaces for a Gaussian stochastic potential with Gaussian autocorrelation function, in one (left) and two (right) dimensions. The depth of the fluctuations is fixed at $H=0.5$, and the correlation lengths are $\sigma=\infty$, 1, 0.5, 0.25, and 0.125.

smaller as the correlation length is reduced and, as the correlation length approaches zero, the spectrum turns into a single Lorentzian line at the position $\omega=0$. This is surprising, since the mean square of the optical density is independent of the correlation length, and is the same as for the classical probability density. For equal correlation lengths, $\sigma^{(2D)}=\sigma^{(1D)}$, the departure of the line shape from the classical limit is much more pronounced in two dimensions than in one dimension. This holds true even for $\sigma^{(2D)}=\sqrt{2}\sigma^{(1D)}$, where all moments of the optical densities are equal up to the third order.[30] This shows that a one-dimensional model gives only a very rough approximation of the line shape in two dimensions.

V. SUMMARY

We have presented a method of calculating optical spectra of semiconductor microstructures which is based upon the evaluation of the electron-hole-pair amplitude in real space and real time. The numerical effort and the storage scale like $O(N)$ with the number of base functions N. Up to prefactors, this is the lowest possible value. The algorithm is even more efficient for the calculation of exciton binding energies, since a much smaller number of grid points is required than for calculating a whole spectrum.

Virtually no errors arise from the time propagation, using the leap-frog scheme, and the accuracy is determined by the matrix representation of the Hamiltonian. The discretization of the Coulomb potential by means of the ground-state wave function provides accurate results, and avoids the calculation of Coulomb matrix elements.

A particular strength of the real-space representation is its flexibility: whereas many previous publications deal only with limiting cases, we are able to cover the whole range of parameters and, therefore, perform transitions, e.g., from thin to thick samples, small to large confinement, and low to high magnetic fields. To increase accuracy and efficiency for particular differential operators and geometries, it is also possible to use mixed bases, made up of finite differences, subband indices, and Fourier coefficients.

To demonstrate the usefulness, we applied the algorithm to calculate the optical spectra of various low-dimensional semiconductors. The examples B–F in Sec. IV are treated for the first time in the whole parameter range.

ACKNOWLEDGMENTS

The authors are indebted to S. Bar-Ad, P. Concus, P.M. Goorjian, N.A. Hill, P. Schmelcher, and K.B. Whaley for stimulating discussions. This work was supported by the Director, Office of Basic Energy Sciences, Division of Material Sciences of the U.S. Department of Energy, under Contract No. DE-AC03-76SF00098. Financial support from the Deutsche Forschungsgemeinschaft (S.G. and F.B.) is gratefully acknowledged.

*Permanent address: Friedrich-Schiller-Universität, Institut für Festkörpertheorie und Theoretische Optik, Max-Wien-Platz 1, 07743 Jena, Germany.

[1] For a review, see, R. Cingolani and R. Rinaldi, Riv. Nuovo Cimento **16**, 1 (1993).
[2] R.J. Elliott, Phys. Rev. **108**, 1384 (1957).
[3] O. Dippel, P. Schmelcher, and L.S. Cederbaum, Phys. Rev. A **49**, 4415 (1994).
[4] H. Chu and Y.-C. Chang, Phys. Rev. B **39**, 10 861 (1989).
[5] R. Zimmermann, Phys. Status Solidi B **135**, 681 (1986).
[6] C.Y.-P. Chao and S.L. Chuang, Phys. Rev. B **43**, 6530 (1991).
[7] G. Wen and Y.-C. Chang, Phys. Rev. B **49**, 16 585 (1994).
[8] D.M. Whittaker, Europhysics Lett. **31**, 55 (1995).
[9] P. Lefebvre, P. Christol, H. Mathieu, and S. Glutsch, Phys. Rev. B **52**, 5756 (1995).
[10] R.D. Richtmyer and K.W. Morton, *Difference Methods for Initial-Value Problems* (Academic, New York, 1967); A.A. Samarskij, *Theorie der Differenzenverfahren* (Geest & Portig, Leipzig, 1984).
[11] Y.I. Shokin, *The Method of Differential Approximation* (Springer, Berlin, 1983).
[12] N. Grün, A. Mühlhans, and W. Scheid, J. Phys. B **15**, 4042 (1982).
[13] For a review, see, R. Kosloff, J. Chem. Phys. **92**, 2087 (1988).
[14] B.M. Deb, P.K. Chattaraj, and S. Mishra, Phys. Rev. A **43**, 1248 (1991).
[15] R. Winkler, Phys. Rev. B **51**, 14 395 (1995).
[16] J.R. Chelikowsky, N. Troullier, and Y. Saad, Phys. Rev. Lett. **72**, 1240 (1994).
[17] S. Schmitt-Rink and D.S. Chemla, Phys. Rev. Lett. **57**, 2752 (1986); I. Balslev, R. Zimmermann, and A. Stahl, Phys. Rev. B **40**, 4095 (1989).
[18] S. Mukamel, *Principles of Nonlinear Optical Spectroscopy* (Oxford University Press, New York, 1995).
[19] N.A. Hill and K.B. Whaley, J. Chem. Phys. **99**, 3707 (1993).
[20] A complete FORTRAN program is available by writing to the first author.
[21] S. Glutsch and D.S. Chemla, Phys. Rev. B **53**, 15 902 (1996).

[22] C. Stafford, S. Schmitt-Rink, and W. Schäfer, Phys. Rev. B **41**, 10 000 (1990).
[23] S. Glutsch, U. Siegner, M.-A. Mycek, and D.S. Chemla, Phys. Rev. B **50**, 17 009 (1994).
[24] S. Bar-Ad *et al.* (unpublished).
[25] K. Brunner, U. Bockelmann, G. Abstreiter, M. Walter, G. Böhm, G. Tränkle, and G. Weimann, Phys. Rev. Lett. **69**, 3216 (1992).
[26] S. Glutsch, P. Lefebvre, and D.S. Chemla (unpublished).
[27] B. Velický and J. Sak, Phys. Status Solidi **16**, 147 (1966).
[28] F.J. Dyson, Phys. Rev. **92**, 1331 (1953); B.I. Halperin, *ibid.* **139**, A104 (1965).
[29] R. Zimmermann, J. Cryst. Growth **101**, 346 (1990); Phys. Status Solidi B **173**, 129 (1992).
[30] S. Glutsch and F. Bechstedt, Superlatt. Microstruct. **15**, 5 (1994).